CHEMISTRY OF MATERIALS
Article

Chem. Mater. **2010,** *22,* 6183–6190 6183
DOI:10.1021/cm102355x

Metallic Pd Nanoparticles Formed by Pd−O−Ce Interaction: A Reason for Sintering-Induced Activation for CO Oxidation

Satoshi Hinokuma,[†,‡] Hiroaki Fujii,[‡] Madoka Okamoto,[‡] Keita Ikeue,[‡] and Masato Machida*[,‡]

[†]*Research Fellow of the Japan Society for the Promotion of Science, and* [‡]*Department of Applied Chemistry and Biochemistry, Graduate School of Science and Technology, Kumamoto University, 2-39-1 Kurokami, Kumamoto, 860-8555 Japan*

Received August 17, 2010. Revised Manuscript Received October 1, 2010

Ambient-temperature CO oxidation activity of Pd/CeO_2 was found to increase by more than 20 times after thermal aging at 900 °C in air. Although the aging resulted in a significant sintering accompanied by a 92% loss of surface area from 92 to 7 $m^2 \cdot g^{-1}$, Pd metal dispersion was preserved at a high value (0.57). The analysis using transmission electron microscopy (TEM), high-angle annular dark-field (HAADF)-scanning transmission electron microscopy (STEM), extended X-ray absorption fine structure (EXAFS), and X-ray photoelectron spectroscopy (XPS) demonstrated that the activation is driven by metal−support interactions followed by phase transformation. Owing to the formation of Pd−O−Ce bonding at the PdO/CeO_2 interface, Pd oxide species are highly dispersed into the surface structure of CeO_2. The Pd oxide becomes unstable when the temperature reaches ≥800 °C, where thermodynamic PdO/Pd phase equilibrium is reached. Finally, the Pd−O−Ce surface moiety is fragmented into metallic Pd particles with a size of 1 to 2 nm, which provide active sites for CO oxidation.

Introduction

Sintering is a main cause of thermally induced deactivation of supported metal catalysts. In many cases, the loss of catalytic surface area caused by metal crystallite growth at elevated temperatures is thermodynamically unavoidable. Two main mechanisms, crystallite migration and atomic/molecular migration, have been known for metal crystallite growth when the temperature is not high enough for vapor transport.[1,2] The crystallite migration involves the migration of metal crystallites over the support surface followed by collision and coalescence. The atomic/molecular migration involves detachment of metal atoms/molecules from crystallites and their migration over the support surface until capture by larger crystallites. The latter mechanism is also used for the explanation of redispersion of supported metals, which emerges for the system enabling strong metal−support bonding. A research group from Toyota has recently reported that the interaction between Pt and CeO_2 at 800 °C under an oxidizing condition causes redispersion of as grown Pt crystallites and, thus, contributes to the sintering inhibition mechanism of Pt/CeO_2.[3,4] The Pt−O−Ce bond formed in an oxidizing atmosphere acts as an anchor and promotes the atomic migration of Pt oxide from the surface of large metallic Pt particles as grown in a reducing atmosphere. Such redispersion is considered to be more difficult when Pt is supported on weakly interacting supports such as γ-Al_2O_3 and SiO_2.[1−4] On the other hand, Newton et al.[5] suggested the occurrence of "oxidationless" promotion of Pd redispersion by O_2 in the gas phase. In case of Pd/γ-Al_2O_3 under forced cycling between CO and NO/O_2 feed, the excess O_2 during the oxidizing part of the cycle causes rapid redispersion of Pd before formal oxidation of Pd^0 to Pd^{2+} is observed. As was proved by these previous studies, metal−support interactions and gas phase O_2 should play a key role in sintering/redispersion phenomena in high-temperature aging of supported metal catalysts.

The use of CeO_2 as a support for precious metals has attracted considerable attention because metal−support interactions allow synergistic oxidation/reduction of both the metal and CeO_2, favoring the catalytic performance in wide applications.[6−8] In this regard, many researchers are recently interested in low-temperature CO oxidation over Pd supported CeO_2.[9−15] The low-temperature activity for

*Corresponding author. Tel/Fax: +81-96-342-3651. E-mail: machida@kumamoto-u.ac.jp.

(1) Wanke, S. E. *Mater. Sci. Res.* **1984**, *16*, 223.
(2) Wanke, S. E.; Flynn, P. C. *Catal. Rev.−Sci. Eng.* **1975**, *12*, 93.
(3) Nagai, Y.; Dohmae, K.; Ikeda, Y.; Takagi, N.; Tanabe, T.; Hara, N.; Guilera, G.; Pascarelli, S.; Newton, M. A.; Kuno, O.; Jiang, H.; Shinjoh, H.; Matsumoto, S. i. *Angew. Chem., Int. Ed.* **2008**, *47*, 9303.
(4) Nagai, Y.; Hirabayashi, T.; Dohmae, K.; Takagi, N.; Minami, T.; Shinjoh, H.; Matsumoto, S. i. *J. Catal.* **2006**, *242*, 103.
(5) Newton, M. A.; Belver-Coldeira, C.; Martínez-Arias, A.; Fernández-García, M. *Angew. Chem., Int. Ed.* **2007**, *46*, 8629.
(6) Trovarelli, A. In *Catalysis by Ceria and Related Materials*; Trovarelli, A., Ed.; Imperial College Press: London, 2002.
(7) Farrauto, R. J.; Heck, R. M. *Catal. Today* **1999**, *51*, 351.
(8) Kaspar, J.; Fornasiero, P.; Graziani, M. *Catal. Today* **1999**, *50*, 285.
(9) Bekyarova, E.; Fornasiero, P.; Kaspar, J.; Graziani, M. *Catal. Today* **1998**, *45*, 179.
(10) Boronin, A. I.; Slavinskaya, E. M.; Danilova, I. G.; Gulyaev, R. V.; Amosov, Y. I.; Kuznetsov, P. A.; Polukhina, I. A.; Koscheev, S. V.; Zaikovskii, V. I.; Noskov, A. S. *Catal. Today* **2009**, *144*, 201.
(11) Fernández-García, M.; Martínez-Arias, A.; Iglesias-Juez, A.; Hungría, A. B.; Anderson, J. A.; Conesa, J. C.; Soria, J. *Appl. Catal., B: Environ.* **2001**, *31*, 39.

Published on Web 10/19/2010

CO oxidation is not typical of Pd catalysts, because strongly oxidized palladium in the form of PdO particles does not show low-temperature catalytic activity.[16−20] Pd catalysts supported on weakly interacting supports such as γ-Al_2O_3 and SiO_2 are more active, but their light-off temperatures are higher than 130−150 °C.[21] The low-temperature activity appears only after deposition of Pd on oxides having variable oxidation states, which enable stronger interactions at the interface. Fernández-García et al.[12] reported that Pd supported on CeO_2-impregnated γ-Al_2O_3 achieves ambient-temperature CO oxidation. They concluded that CeO_2 not only promotes the formation of metallic Pd efficient for CO activation but also yields reactive vacancies efficient for O_2 activation at the Pd−CeO_2 interface. Boronin et al.[10] recently reported that ambient temperature activity to CO oxidation could be achieved by Pd supported on CeO_2 alone, which was characterized by highly dispersed Pd consisting of the surface interaction phase ($Pd_xCeO_{2-\delta}$) and very small Pd metal clusters (< 1 nm). The formation of PdO−CeO_2 composite oxides has also been proposed by several researchers,[22,23] but these phases could not be isolated for the structural characterization. In this way, CO oxidation is a useful indicator of the metal−support interaction of Pd/CeO_2 catalyst. However, the Pd/CeO_2 catalysts in these previous works are calcined at relatively low temperatures (≤600 °C). When Pd is supported on sintered CeO_2 (≤800 °C) and/or Pd-supported Ce oxide is sintered at high temperatures, the activity at ambient temperature is considered to decrease to a significant extent.[10,24] To avoid formation of sintered aggregates of Pd, CeO_2-encapsulated Pd having core−shell nanostructures has been recently synthesized using a microemulsion approach.[25,26]

In this paper, we demonstrate an exceptional case that significant thermal sintering of Pd-supported CeO_2 in the presence of O_2 converts it to be a very active catalyst for CO oxidation working at ambient temperature. This unusual phenomenon is considered to be associated with interactions at the interface between Pd and CeO_2, because other catalysts, such as Pd/γ-Al_2O_3 and Pt/CeO_2, after the same aging showed a considerable deactivation. The reason for the sintering-induced activation is discussed on the basis of local structural analysis by the use of transmission electron microscopy (TEM)/high-angle annular dark-field (HAADF)-scanning transmission electron microscopy (STEM), X-ray absorption fine structure (XAFS), X-ray photoelectron spectroscopy (XPS), and Fourier transform infrared (FT-IR) with intention of expanding the knowledge of applying this phenomenon broadly to precious metal catalysts.

Experimental Section

Materials. High purity CeO_2 (Rhodia Ltd., 99.99%) was used as a support material. The Pd/CeO_2 catalyst with a loading of 0.4% as Pd metal by mass was prepared by a conventional wet impregnation method using aqueous solutions of $Pd(NO_3)_2$ (Tanaka Kikinzoku Kogyo, 99.0%) and subsequent heating at 600 °C for 3 h in air. For extended X-ray absorption fine structure (EXAFS) measurement described below, the catalysts with a high loading of 2.0% by mass were used to ensure a good quality signal. As-prepared catalyst was thermally aged in a flow of 10% H_2O in air at 700−1000 °C for 25 h. The aging was also carried out in streams of dry air, He, and 5% H_2 in He at 900 °C for 25 h.

Characterization. Powder X-ray diffraction (XRD) measurement was performed using monochromated Cu Kα radiation (30 kV, 20 mA, Rigaku Multiflex). The loading of Pd was analyzed by X-ray fluorescence measurement (Horiba-MESA500). A FEI TECNAI F20 transmission electron microscope operating at 200 kV was used to obtain high-resolution transmission electron microscope images. HAADF-STEM was carried out using Hitachi HD-2700 Cs-corrected STEM operating at 200 kV. The beam size was 0.2 nm for HAADF-STEM and 0.3 nm for energy dispersive X-ray (EDX) analysis. The XPS spectra were measured on a VG Sigmaprobe spectrometer using Mg Kα radiation (15 kV, 20 mA). The metal dispersion of Pd (D_{Pd}) was determined after reduction treatment by the modified pulsed CO technique developed by Takeguchi et al.[27] The method uses preinjection of CO_2 to prevent overestimation of D_{Pd} caused by CO adsorption on CeO_2 as the carbonate species. First, the Pd/CeO_2 sample was heated in a stream of O_2 at 300 °C for 10 min and subsequently cooled down to 50 °C where the sample was flushed with He for 5 min. Next, the sample was heated in a stream of 5% H_2/Ar during temperature ramp of 10 °C·min^{-1} to 200 °C. After cooling down to 50 °C, the sample was exposed to flows of gases in the following sequence of steps: (i) He (5 min); (ii) O_2 (5 min); (iii) CO_2 (10 min); (iv) He (20 min); (v) 5% H_2/He (5 min). Finally, CO was pulsed every 2 min in a stream of He until the adsorption onto the sample is to be saturated.

Measurement of X-ray absorption spectra of Pd at the K edge was performed on the NW10A station of Photon Factory for Advanced Ring (PF-AR), High Energy Accelerator Research Organization (KEK) at Tsukuba (Proposal No. 2009G574). A Si (311) double-crystal monochromator was used. Pd K-edge spectra were recorded at ambient temperature in a transmission mode using ionization chambers filled with 100% Ar for an incident beam and of 100% Kr for a transmitted beam. A reference sample (PdO, 0.06 g) was mixed with boron nitride (BN) powders (0.14 g) to give an appropriate absorbance at the

(12) Fernández-García, M.; Martínez-Arias, A.; Salamanca, L. N.; Coronado, J. M.; Anderson, J. A.; Conesa, J. C.; Soria, J. *J. Catal.* **1999**, *187*, 474.
(13) Pozdnyakova, O.; Teschner, D.; Wootsch, A.; Kröhnert, J.; Steinhauer, B.; Sauer, H.; Toth, L.; Jentoft, F. C.; Knop-Gericke, A.; Paál, Z.; Schlögl, R. *J. Catal.* **2006**, *237*, 17.
(14) Wilson, E. L.; Chen, Q.; Brown, W. A.; Thornton, G. *J. Phys. Chem. C* **2007**, *111*, 14215.
(15) Zhu, H.; Qin, Z.; Shan, W.; Shen, W.; Wang, J. *J. Catal.* **2004**, *225*, 267.
(16) Bourane, A.; Bianchi, D. *J. Catal.* **2004**, *222*, 499.
(17) Bowker, M.; Jones, I.; Bennett, R.; Esch, F.; Baraldi, A.; Lizzit, S.; Comelli, G. *Catal. Lett.* **1998**, *51*, 187.
(18) Oh, S.-H.; Hoflund, G. B. *J. Phys. Chem. A* **2006**, *110*, 7609.
(19) Oh, S.-H.; Hoflund, G. B. *J. Catal.* **2007**, *245*, 35.
(20) Penner, S.; Bera, P.; Pedersen, S.; Ngo, L. T.; Harris, J. J. W.; Campbell, C. T. *J. Phys. Chem. B* **2006**, *110*, 24577.
(21) Bera, P.; Patil, K. C.; Jayaram, V.; Subbanna, G. N.; Hegde, M. S. *J. Catal.* **2000**, *196*, 293.
(22) Priolkar, K. R.; Bera, P.; Sarode, P. R.; Hegde, M. S.; Emura, S.; Kumashiro, R.; Lalla, N. P. *Chem. Mater.* **2002**, *14*, 2120.
(23) Colussi, S.; Gayen, A.; Farnesi Camellone, M.; Boaro, M.; Llorca, J.; Fabris, S.; Trovarelli, A. *Angew. Chem., Int. Ed.* **2009**, *48*, 8481.
(24) Martínez-Arias, A.; Fernández-García, M.; Iglesias-Juez, A.; Hungría, A. B.; Anderson, J. A.; Conesa, J. C.; Soria, J. *Appl. Catal., B: Environ.* **2002**, *38*, 151.
(25) Cargnello, M.; Montini, T.; Polizzi, S.; Wieder, N. L.; Gorte, R. J.; Graziani, M.; Fornasiero, P. *Dalton Trans.* **2010**, *39*, 2122.
(26) Cargnello, M.; Wieder, N. L.; Montini, T.; Gorte, R. J.; Fornasiero, P. *J. Am. Chem. Soc.* **2009**, *132*, 1402.
(27) Takeguchi, T.; Manabe, S.; Kikuchi, R.; Eguchi, K.; Kanazawa, T.; Matsumoto, S.; Ueda, W. *Appl. Catal., A: Gen.* **2005**, *293*, 91.

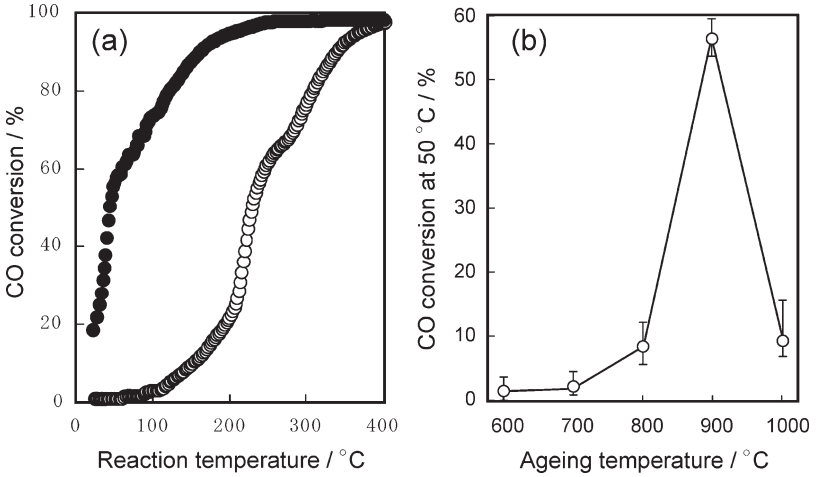

Figure 1. (a) Light-off of a stream of 0.1% CO and 1.25% O_2 balanced with He for Pd/CeO_2 before (○) and after (●) aging at 900 °C in 10% H_2O/air. (b) CO conversion to CO_2 at 50 °C as a function of aging temperature. Error bars correspond to the maximum and minimum values in two or three runs of the catalytic reaction.

edge energy, whereas other samples (0.2 g) were used without mixing with BN. The XAFS data were processed by a REX 2000 program (Rigaku). EXAFS oscillation was extracted by fitting a cubic spline function through the postedge region. The k^3-weighted EXAFS oscillation in the 3.0−16.0 $Å^{-1}$ regions was Fourier transformed. Pd foil and PdO were used as references in order to extract the amplitude and phase shift function for Pd−Pd and Pd−O bonds. Coordination number (CN), interatomic distance (r), and ΔE_0 were fitted, and Debye−Waller factors were fixed. Plots of the FT module/imaginary part of both experimental and fitting results are included in Supporting Information (Figure S1).

Catalytic Reactions. A catalytic reaction test for CO oxidation was carried out in a flow microreactor at atmospheric pressure. A granule catalyst (50 mg, 10−20 mesh) was fixed in a quartz tube (ϕ6 mm) by quartz wool at both ends of a catalyst bed. Temperature dependence of catalytic activity was evaluated by heating the catalyst bed from ambient temperature to 600 °C at constant rate of 10 °C·min^{-1} by supplying a gas mixture containing CO (0.1%), O_2 (1.25%), and He (balance) supplied at 100 $cm^3 \cdot min^{-1}$ ($W/F = 5.0 \times 10^{-4}$ g·min·cm^{-3}). The effluent gas was analyzed using a Pfeiffer GSD30101 mass spectroscopy and a Horiba VA3000 NDIR CO/CO_2 gas analyzer.

In situ FT-IR spectroscopy was conducted on a Nicolet 6700 spectrometer and a temperature-controllable diffuse reflectance reaction cell with a KBr window that was connected to a gas supply system to allow measurement under controlled gas environments at atmospheric pressure. The sample was finely ground and placed in a crucible inside the cell to be exposed to a flowing gas mixture. The sample was first preheated in situ in a flowing He at 200 °C for 1 h prior to any experiment. This was followed by cooling to 50 °C, purging with He, and subsequent admission of gas mixtures of 1% CO and He balance for 30 min. Immediately following this procedure, the cell was flushed with a stream of He for 5 min at 50 °C, where spectrum was taken in a stream of He and after subsequent supply of 2.5% O_2/He for 10 min at the same temperature.

Results and Discussion

Effect of Thermal Aging on Catalytic Activity of Pd/CeO_2. Figure 1a exhibits the temperature dependences of CO conversion to CO_2 before and after thermal aging at 900 °C. As-prepared Pd/CeO_2 initiated the reaction at around 100 °C and achieved the complete conversion at 400 °C. Because CeO_2 alone could attain the CO conversion of less than 15% at 400 °C, the activity of the present catalyst depends on Pd species. It should be noted that the activity was significantly enhanced after thermal aging in steam/air at 900 °C, enabling the light-off to take place even at ambient temperature. The enhancement of catalytic activity was observed for CO oxidation not only under an oxygen-excess condition (Figure 1) but also under a stochiometric condition (0.1% CO and 0.05% O_2 balanced with He, Supporting Information, Figure S2). As shown in Figure 1b, which plots the CO conversion measured at 50 °C versus the aging temperature, the appearance of the low-temperature activity required aging at 900 °C, but it was deteriorated by further heating at 1000 °C. The active phase once formed by thermal aging at 900 °C was so stable that the low-temperature activity could be preserved after repetition of the catalytic test in a light-off mode and/or a steady state mode at 50 °C.

Table 1 compares S_{BET} and D_{Pd} of Pd/CeO_2 after thermal aging at elevated temperatures. The XRD patterns showed that diffraction peaks of CeO_2 became sharp and strong with an increase of temperature. The loading of Pd did not change after thermal aging up to 1000 °C. It should be noted that D_{Pd} was preserved as high as 0.57 even after aging at 900 °C in contrast to a significant decrease of S_{BET} from 92 to 7 $m^2 \cdot g^{-1}$. This is not the case of a reference catalyst, 0.4 mass% Pd/γ-Al_2O_3; D_{Pd} decreased steeply from 0.25 to 0.05 when S_{BET} decreased from 121 to 71 $m^2 \cdot g^{-1}$. The effect of thermal aging on catalytic activity was also examined under various gas streams including O_2, H_2, He, and H_2O at 900 °C (Supporting Information, Figure S3). The most significant enhancement of activity was observed only when the aging was carried out in the presence of O_2. In contrast, less significant effects were observed for He and H_2. Adding water vapor (10% by volume) into air or He slightly promoted catalyst sintering but its effect was not essential. When Pd was supported on other oxide

Table 1. Brunauer-Emmett-Teller (BET) Surface Area, Metal Dispersion, and Oxidation State of Pd/CeO_2

aging[a]/°C	$S_{BET}/m^2 \cdot g^{-1}$	D_{Pd}[b]	$Pd^0/(Pd^0 + Pd^{2+})$[c]
none	92	0.96	0
700	89	0.77	0
800	37	0.80	0
900	7	0.57	0.11
1000	5	0.47	0.18

[a] Aging for 25 h. [b] Determined by pulsed CO chemisorption after H_2 reduction at 200 °C. [c] Determined by Pd3d XPS spectra.

supports such as γ-Al_2O_3 and SiO_2 or Pt was supported on CeO_2, rapid deactivation was caused by thermal aging in air (Supporting Information, Figure S4). These results suggest that the efficient activation occurs in the catalyst based on combination between Pd and CeO_2 only when the thermal aging at around 900 °C is applied.

Local Structure of Thermally Aged Pd/CeO_2. In order to gain insight into the beneficial effect of thermal aging on the catalytic activity of Pd/CeO_2, a local structural analysis by electron microscopy was carried out. TEM images of Pd/CeO_2 before and after thermal aging are compared in Figure 2. As-prepared catalyst was composed of CeO_2 particles smaller than 10 nm. This is consistent with the mean particle size of CeO_2, which was calculated from S_{BET} ($92\ m^2 \cdot g^{-1}$) to be about 9 nm on the assumption of a spherical crystallite. In the bright-field TEM images, it was difficult to discriminate Pd/PdO particles from the background of CeO_2 particles having a high contrast. This is indicative of high dispersion of Pd species on the surface structure CeO_2, which is in accordance with the very high D_{Pd} (0.96) in Table 1. In contrast, thermally aged Pd/CeO_2 (Figure 2b) consisted of much larger grains of CeO_2 (> 100 nm) and exhibited neck growth as a consequence of sintering. Again, Pd/PdO particles could not be identified in the bright field image.

The structure of Pd species formed on the aged catalyst was next characterized using HAADF-STEM, which is a powerful technique suited for *Z*-contrast images (*Z*: the atomic number), because the intensity of scattered electrons in the mode is proportional to Z^2.[28,29] The scattering intensity is also proportional to the thickness of particles. Therefore, Pd metal and/or oxide should appear as bright spots on the matrix of CeO_2 support. Figure 3a,b shows bright-field STEM and HAADF-STEM images, respectively, taken from a same position in Pd/CeO_2 after thermal aging at 900 °C. As in the case of Figure 2b, thin crystallites adhering to the surface of large CeO_2 grains were frequently observed as shown by an arrow ① (panel b). However, the parallel EDX analysis (panel d) at the point with a probe size of 0.3 nm did not show the presence of Pd. An enlarged HAADF-STEM image (panel c) of the square region in panel a exhibits the presence of finely dispersed nanoparticles with a slightly bright contrast as is shown by an arrow ②, and the EDX spectrum clearly showed the presence of Pd (panel d). The size of these particles in the range of 1 to 2 nm

(28) Nellist, P. D.; Pennycook, S. J. *Science* **1996**, *274*, 413.
(29) Treacy, M. M. J.; Rice, S. B. *J. Microsc.* (*Oxford, United Kingdom*) **1989**, *156*, 211.

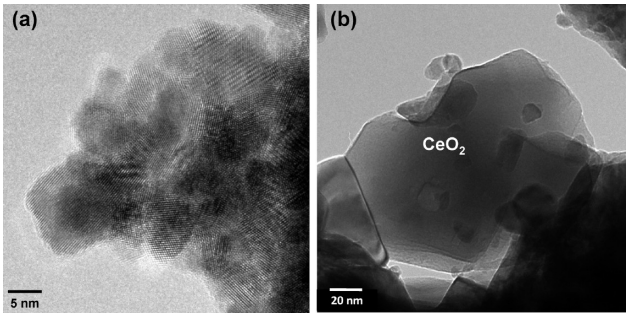

Figure 2. TEM images of Pd/CeO_2 (a) before and (b) after aging at 900 °C in 10% H_2O/air.

is very similar to the diameter of metallic Pd particles, 2 nm, which was calculated from $D_{Pd} = 0.57$ in Table 1. It should be noted that such very small Pd particles with single nanometer size could survive after significant sintering of CeO_2 during thermal aging at as high as 900 °C. As described later, these nanoparticles seem to be composed of metallic Pd.

The local structure around Pd was next investigated by XAFS. The Pd loading for this measurement was increased to 2.0 mass%, but changes in the catalytic property upon thermal aging were consistent with those of 0.4 mass% Pd/CeO_2 (Supporting Information, Figure S5). The XAFS data of 2.0 mass% Pd is, therefore, a reasonable measure for evaluating the local structure of 0.4 mass% Pd/CeO_2. Figure 4 shows the Fourier transforms of k^3-weighted Pd K-edge EXAFS of Pd/CeO_2 before and after aging at elevated temperatures together with two references (Pd foil and PdO). Because these spectra were not corrected for phase shifts, the observed peaks are shifted to a lower *r*-value from true interatomic distances. When the first and second coordination shells were filtered, the best curve-fitting was obtained and the resultant structural parameters including the phase shift corrected *r*-value are shown in Table 2. For all of the Pd/CeO_2 samples before and after aging at different temperatures (a−d), the first coordination shell indicated an intense peak attributable to the Pd−O bond. The curve-fitting analysis of the first coordination shell yielded CN of about 4 and *r* of about 2 Å as in the case of bulk PdO. Unlike PdO alone (f), however, Pd−O−Ce with 3.18 Å appeared in the second shell of the as-prepared sample (a) instead of Pd−O−Pd with 3.04 Å. Considering the lack of a Pd−O−Pd shell and CN of Pd−O (4.2) close to that of Pd−O−Ce (3.2), a large part of Pd should be present in a form of the Pd−O−Ce moiety.

As is evident from Figure 4 and Table 2, the Pd−O−Ce shell became less intense with an increase of aging temperature up to 900 °C and finally disappeared at 1000 °C, where the appearance of Pd−O−Pd with CN close to 4 indicated the deposition of bulk PdO. In addition, a Pd−Pd shell appeared at 900 °C and became intense at 1000 °C. These results demonstrate that the Pd−O−Ce moiety is stable up to around 800 °C under the atmospheric O_2 pressure. Above this temperature, the Pd−O−Ce moiety would be dissociated to form metallic Pd species. The Pd−O−Ce moiety could be detected for Pd/CeO_2 only after aging under oxidizing and/or an inert

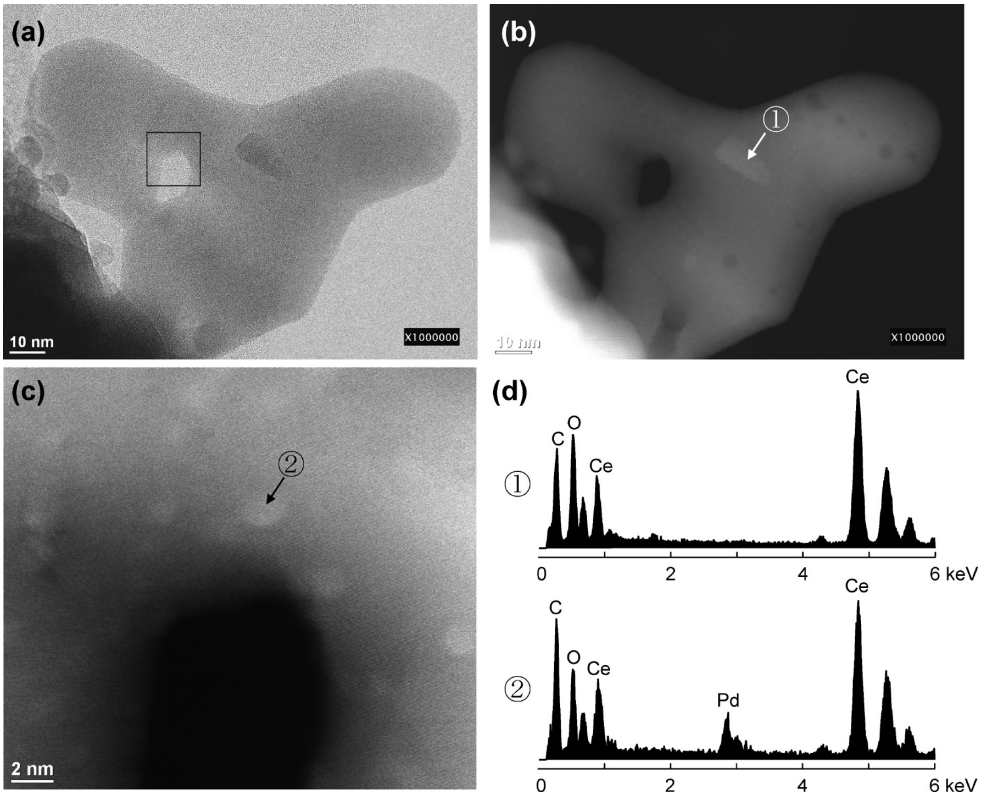

Figure 3. (a) A bright-field STEM image and (b) a corresponding HAADF-STEM image of Pd/CeO_2 after aging at 900 °C in 10% H_2O/air; (c) a HAADF-STEM image taken from a square region in (a); (d) EDX spectra taken from positions shown by arrows ① and ②.

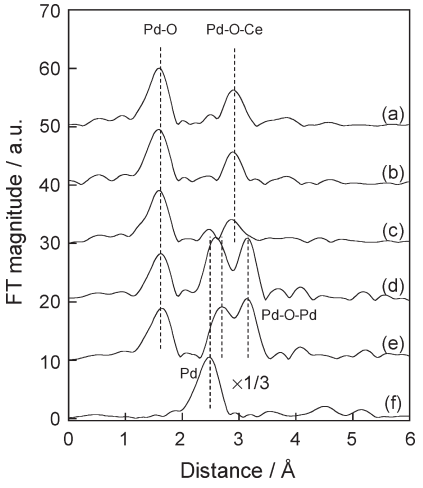

Figure 4. Fourier transforms of k^3-weighted Pd K-edge EXAFS of Pd/CeO_2 (a) before and after aging at different temperatures: (b) 800 °C, (c) 900 °C, and (d) 1000 °C and references; (e) PdO and (f) Pd foil.

atmosphere (O_2, air, and He; Supporting Information, Table S1). On the other hand, CN of the Pd−Pd shell exhibited the following sequences of increasing number: O_2 (0.47) ~ air (0.51) < He (2.4) < H_2/He (10.8), suggesting rapid growth as bulk Pd metals with decreasing equilibrium oxygen pressure (pO_2). The highest catalytic activity of metallic Pd formed in the presence of O_2 should, therefore, be originated from its very small particle size as observed by HAADF-STEM (Figure 3).

The variation of Pd oxidation state with thermal aging in air was also observed by XPS. Figure 5 shows the XPS spectra of the Pd 3d region before and after aging of Pd/CeO_2 at 900 °C. The peaks observed for as-prepared sample were fitted with one set of spin−orbit doublets of $3d_{5/2}$ (337.6 eV) and $3d_{3/2}$ (342.8 eV), indicating that Pd is present mostly in the Pd^{2+} state. However, these values are higher than those reported for bulk PdO (336.8 and 342.2 eV) and close to those of $PdCl_2$ and $Pd(NO_3)_2$.[30,31] Priolkar et al.[22] reported such a higher shift of Pd^{2+} XPS signals for their solution combustion-synthesized Pd/CeO_2, which contains a Pd−O−Ce bonding in a pseudo solid solution phase. They proposed that Pd^{2+} in the higher ionic state is stabilized in the Ce^{3+} site leading to a strong interaction via Pd−O−Ce bonding. Similar spectra consisting of Pd^{2+} alone were obtained for the present Pd/CeO_2 aged at ≤800 °C. In contrast, the spectra taken after aging at 900 °C could be resolved into two sets of spin−orbit doublets, which were attributed to Pd^{2+} (337.9 and 342.8 eV) and Pd^0 (335.3 and 340.3 eV). The calculated fraction of Pd^0 is shown in Table 1. The presence of Pd^0 was negligible at temperatures ≤800 °C, where the oxide form is thermodynamically stable. At higher temperatures, ≥900 °C, Pd^0 increased monotonically, but the growth of Pd metal particles as well as Pd oxide particles is evident from increased CN of Pd−Pd and Pd−O−Pd shells in EXAFS results (Table 2). The effect of thermal aging on Ce 3d and O 1s XPS spectra was not obvious.

(30) Brun, M.; Berthet, A.; Bertolini, J. C. *J. Electron Spectrosc. Relat. Phenom.* **1999**, *104*, 55.
(31) Pillo, T.; Zimmerman, R.; Steiner, P.; Hufner, S. *J. Phys.: Condens. Matter* **1997**, *9*, 3987.

Table 2. Fitting Parameters Obtained from Pd K-Edge EXAFS Analysis of Pd/CeO_2 after Aging in Air at Different Temperatures for 25 h[a]

samples	shell	CN[b] (±0.2)	r/Å[c] (±0.03)	$\sigma^2/10^{-2}$ Å^{2}[d] (±0.05)	R/%
Pd/CeO_2 (as-prepared)	Pd−O	4.2	1.98	0.48	0.2
	Pd−O−Ce	3.2	3.18	0.64	2.6
Pd/CeO_2 (800 °C)	Pd−O	4.1	1.98	0.48	0.3
	Pd−O−Ce	2.7	3.16	0.61	1.6
Pd/CeO_2 (900 °C)	Pd−O	3.8	1.99	0.48	1.7
	Pd−Pd	0.51	2.75	0.61	0.7
	Pd−O−Ce	1.9	3.14	0.61	0.7
Pd/CeO_2 (1000 °C)	Pd−O	3.5	2.00	0.48	0.4
	Pd−Pd	1.2	2.75	0.61	0.5
	Pd−O−Pd	3.7	3.04	0.58	0.5
	Pd−O−Pd	8.0	3.42	0.67	0.5
Pd foil	Pd−Pd	12.0	2.75	0.61	2.5
PdO	Pd−O	4.0	2.02	0.48	4.0
	Pd−O−Pd	4.0	3.04	0.58	1.2
	Pd−O−Pd	8.0	3.42	0.67	1.2

[a] Interval of k-space to r-space of FT is 3.0−16.0 Å^{-1}. [b] Coordination number. [c] Atomic distance. [d] Debye−Waller factor.

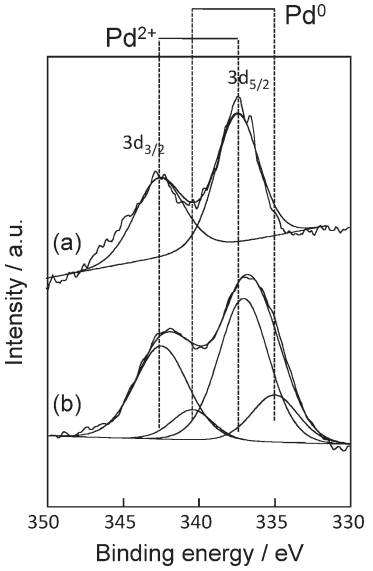

Figure 5. Pd3d XPS spectra of Pd/CeO_2 (a) before and (b) after aging at 900 °C in 10% H_2O/air.

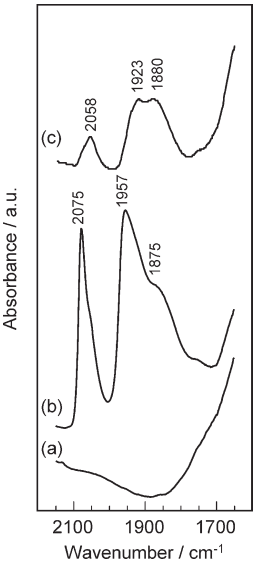

Figure 6. IR spectra of CO absorbed on Pd/CeO_2 at 50 °C (a) before and (b) after aging at 900 °C in 10% H_2O/air. The spectrum (c) was measured after CO adsorption followed by O_2 admission at 50 °C.

CO Adsorption. To check the correlation between local structural change and catalytic activity, in situ infrared spectra of CO adsorbed on as-prepared and as-aged Pd/CeO_2 was measured without further reduction pretreatment. Figure 6 shows the spectra in the range of CO stretching vibration mode. The spectrum for as-prepared catalyst showed no obvious bands in the region of 1650−2150 cm^{-1} in accordance with the absence of catalytic CO oxidation at this temperature (50 °C). The chemisorption of CO onto fully oxidized Pd surface seems to be negligible at this temperature. The catalyst after aging, however, showed three strong absorption bands assigned to linear (2075 cm^{-1}) and bridged (1957 and 1875 cm^{-1}) CO species adsorbed onto metallic Pd.[12,32] Subsequent exposure to O_2 caused a substantial decrease in intensities and shifts to lower wavenumbers (2058 and 1923 cm^{-1}) of the first and second bands as a consequence of the CO−O_2 reaction. The shift seems to correlate with a decrease in CO coverage on the Pd surface.[11] These results clearly demonstrate that the metallic Pd nanoparticles are essential for the low-temperature CO oxidation over the thermally aged Pd/CeO_2.

Reasons for Activation by Thermal Aging. With all these results taken into consideration, a mechanism for the activation caused by high-temperature air-aging is considered as follows (Figure 7). First, the formation of Pd−O−Ce bonding at the PdO/CeO_2 interface allows high dispersion of Pd oxide into the surface structure of sintered CeO_2 crystallites. Such local Pd−O−Ce interactions with different structural models have been already reported by several research groups.[22,23,33,34] Priolkar et al.[22] reported Pd K-edge EXAFS data of $Ce_{0.99}Pd_{0.01}O_{1.90}$ solid solutions prepared by the solution−combustion method. They observed the third shell at r = 3.31 Å having

(32) Fernandez-Garcia, M.; Anderson, J. A.; Haller, G. L. *J. Phys. Chem.* **1996**, *100*, 16247.
(33) Hosokawa, S.; Taniguchi, M.; Utani, K.; Kanai, H.; Imamura, S. *Appl. Catal., A: Gen.* **2005**, *289*, 115.
(34) Matsumura, Y.; Shen, W.-J.; Ichihashi, Y.; Okumura, M. *J. Catal.* **2001**, *197*, 267.

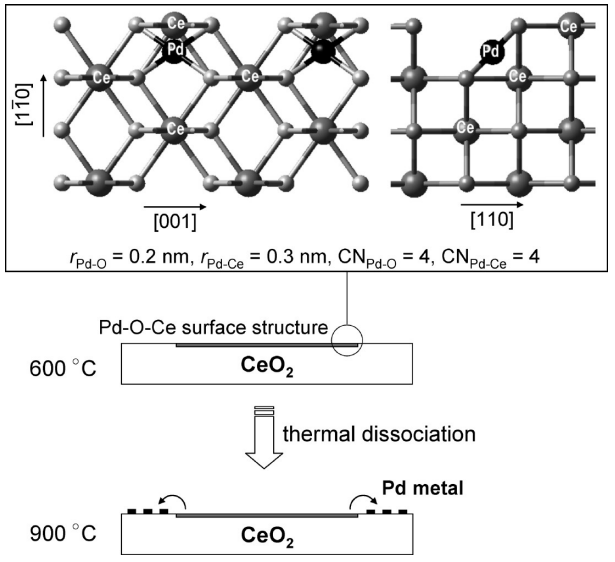

Figure 7. Possible mechanism of sintering-induced activation of Pd/CeO_2. The surface Pd−O−Ce superstructure on CeO_2 (110) proposed by Colussi et al.[23] is shown as an inset. One Pd and its four nearest Ce are highlighted.

CN = 7.3, which was attributed to Pd^{2+} occupied in the eight-folded Ce site in bulk CeO_2. Therefore, this solid solution model is not suitable for the Pd−O−Ce bonding with CN = 3.2 in the present study (as-prepared, Table 2). More recently, Colussi et al.[23] reported the formation of Pd−O−Ce surface superstructure in Pd/CeO_2 as revealed by density-functional theory (DFT) calculations on the basis of high-resolution TEM data. The model consists of a square-planar PdO_4 unit, Pd of which is coordinated by two O atoms of the top layer of the CeO_2 (110) surface and by two O atoms of the second layer (see an inset in Figure 7). The resulting local coordination of Pd−O (r = ~2 Å, CN = 4) and Pd−O−Ce (r = ~3 Å, CN = 4) is consistent with the present EXAFS data of as-prepared Pd/CeO_2 (Table 2). Therefore, Pd−O−Ce with a square-planar geometry is a possible structure candidate of the present system.

The strong Pd−O−Ce interaction is also proved by the fact that thermal aging at ≤800 °C results in only a slight decrease in D_{Pd} (Table 1). The surface Pd oxide species themselves should not be an active site for low-temperature CO oxidation. The Pd−O−Ce moiety becomes instable with an increase of aging temperature (≥800 °C). Finally, at 900 °C, the PdO/Pd phase equilibration causes the thermodynamic dissociation of Pd oxide species to yield a number of metallic Pd nanoparticles capable of activating CO. Because the thermodynamic dissociation temperature of PdO is about 750 °C at P_{O2} = 0.2 bar, the present Pd−O−Ce moiety should be more stable than PdO alone. Unlike the present system, Pd supported on γ-Al_2O_3 as a weakly interacting support yielded large metallic Pd particles (D_{Pd} = 0.05) with a low catalytic activity after thermal aging.

Considering the metallic Pd nanoparticles in intimate contact with CeO_2 as an active site, a question may arise on the effect of reduction treatment on the present Pd/CeO_2 catalyst. As described above, thermal aging in 5% H_2/He at 900 °C could not enhance the activity (Supporting Information, Figure S3), probably because the temperature is too high to keep metallic Pd in nanometer sizes. In addition, it is known that severe reduction treatment of Pd/CeO_2 suppress the CO chemisorption, probably because of metal decoration and/or electronic transfer effects of reduced CeO_2.[35] However, when we performed the H_2 reduction treatment of as-prepared Pd/CeO_2 under milder conditions (200−400 °C), we could observe the enhanced CO oxidation activity (Supporting Information, Figure S6). The improved activity can be related to the deposition of metallic Pd nanoparticles having optimum electronic and geometrical structure for CO oxidation. Boronin et. al[10] pointed out another effect of H_2 treatment, which yields hydroxyl on the surface of CeO_2 along the boundary with Pd. They can react with CO to form intermediates such as hydocarbonate and formate species. However, no significant formation of such hydroxyls was found in the present thermally aged Pd/CeO_2 having the highest activity for CO oxidation.

An interesting fact we found in the present work is that high dispersion of Pd could be preserved on CeO_2 grains even after significant thermal sintering, because the strong Pd−O−Ce interaction on the (110) surface of CeO_2 causes an anchoring effect. In this sense, the morphology in terms of exposed crystal face of CeO_2 is very important. Our TEM observation (Figures 2 and 3) clearly demonstrates significant grain growth of CeO_2 after thermal aging at 900 °C. However, CeO_2 particles exhibited irregular shapes, and a distinguishable change in morphology could not be detected after thermal aging. According to previous studies[36,37] on CeO_2 nanoparticles, low index surfaces of CeO_2 such as (111) and (110) should be exposed on the surface and the (110) surface is considered to play a key role in catalysis. These considerations suggest that the formation of metallic Pd nanoparticles on the CeO_2 (110) surface is a primary factor for the present sintering-induced activation. The possibility of sintering-induced activation of supported metal catalysts opens exciting perspectives in the development of efficient and robust catalysts especially in high-temperature processes including environmental applications.

Conclusion

The present study shows that the thermal aging at 900 °C in air can activate the Pd/CeO_2 catalyst for low-temperature CO oxidation, in complete contrast to other supported catalysts such as Pd/γ-Al_2O_3 and Pt/CeO_2, which are deactivated by sintering. The strong metal−support interaction via Pd−O−Ce bonding prevents the sintering of Pd oxide species at ≤800 °C and deposits metallic Pd particles with a size of 1 to 2 nm, when the aging temperature reaches

(35) Wieder, N. L.; Cargnello, M.; Bakhmutsky, K.; Montini, T.; Fornasiero, P.; Gorte, R. J. J. Phys. Chem. C **2010**, DOI:10.1021/jp102965e.
(36) Sayle, T. X. T.; Parker, S. C.; Catlow, C. R. A. *Surf. Sci.* **1994**, *316*, 329.
(37) Yang, Z.; Woo, T. K.; Baudin, M.; Hermansson, K. *J. Chem. Phys.* **2004**, *120*, 7741.

to the equilibrium of PdO/Pd phase transformation. The metallic Pd nanoparticles in intimate contact with CeO_2 are responsible for CO adsorption and following reactions with oxygen near room temperature.

Acknowledgment. This study was supported by Elements Science and Technology Project from the Ministry of Education, Culture, Sports, Science, and Technology. XAFS experiments were carried out on NW10A of Photon Factory, High Energy Accelerator Research Organization (KEK) (Proposal No. 2009G574).

Supporting Information Available: Additional figures of the FT module/imaginary part of both experimental and fitting results for Pd K-edge EXAFS and of light-off characteristics and a table of the fitting parameters obtained from Pd K-edge EXAFS analysis (PDF). This material is available free of charge via the Internet at http://pubs.acs.org.